Report No.
UCB/SEMM-2011/01

Structural Engineering
Mechanics and Materials

NONLINEAR CYCLIC TRUSS MODEL FOR STRENGTH DEGRADING REINFORCED CONCRETE PLANE STRESS ELEMENTS

By

Marios Panagiotou, and José I. Restrepo

February 2011

Department of Civil and Environmental Engineering
University of California, Berkeley

ABSTRACT

This report describes a nonlinear truss modeling approach for reinforced concrete walls, or in general, for plane stress reinforced concrete elements subjected to cyclic reversals. Nonlinear vertical, horizontal, and diagonal truss elements are used to represent concrete and steel reinforcement. Here, the flexure-shear interaction is intrinsically modeled. The model captures the strain histories in the reinforcement and in the concrete and accounts for the dependency of the concrete stress-strain relationship in compression on the transverse strain, including stiffness and strength degradation. The model considers also mesh size effects. The capabilities of the model are demonstrated by comparing the measured and computed cyclic response of five test walls, which displayed significant flexure-shear interaction, including a six-story wall with openings.

INTRODUCTION

Computation of the nonlinear cyclic response of reinforced concrete (RC) walls to earthquake excitation is an area of significant interest to both practicing engineers and researchers. This task is especially challenging when the response of a RC wall is affected significantly by flexure-shear interaction (FSI) and the wall is subjected to a load history involving multiple large amplitude cyclic reversals. Combination of axial, flexural, and shear load on a component results in a multi-axial stress state, which in turn leads to coupling of nonlinearities due to flexure (bending moment and axial load), and shear, referred as FSI. FSI strongly affects the cyclic behavior of RC walls in terms of strength, stiffness, deformation capacity, softening response, and strains developed in steel and concrete. For this reason, guidelines for the assessment of the force and deformation capacity of these members, see for example FEMA 273[1] and FEMA 356,[2]

are given by backbone formulations that are load-history invariant. Testing of reinforced concrete columns[3] and walls[4] has shown that the shear strength and the onset of strength degradation depend on the load history. The model described in this report considers the effects of load history on structural response.

This report describes a nonlinear truss modeling approach for reinforced concrete walls, or in general, for plane stress reinforced concrete elements subjected to cyclic reversals of increasing displacement amplitude. The main objective of the model is to compute the post cracking plane stress behavior, the lateral force, and deformation capacity of RC walls with significant flexure shear interaction including softening. The approach requires a computer to be implemented. The model approximates well FSI and recognizes the effect of the transverse strain on the stress-strain relationship of concrete in compression as reported by Vecchio and Collins in their development of the Modified Compression Field Theory,[5] but makes the transverse strain reduction factor a function of the gage length as explained below. In relation with previous truss models, this model: i) uses a parallel angle truss model, ii) accounts for tension stiffening also in the horizontal direction and iii) accounts for mesh size effects to determine an appropriate stress-strain relationship for concrete. The capabilities of the model are demonstrated by comparing the measured and computed response of five test units. The first, third, and fifth test units are characterized by significant flexure-shear interaction in the response while the second and fourth units have a shear critical response. The global response, in terms of lateral force-lateral displacement is presented for all cases as well as the strain response of some regions for the first test unit. The more localized response of diagonal concrete elements is also discussed in all cases.

Practicing engineers and researchers need computational tools that compute accurately the cyclic response of RC walls, and, in particular, force and deformation capacities and their materials strains. Such assessment can be done either with simplified and empirical models or with refined finite element (FE) models. An engineering tool of intermediate complexity, in comparison with finite element models, is presented in this report. This tool requires less computational effort and time than FE methods, using nonlinear truss elements with the added advantage that by using truss elements the user gets a feeling of the internal force. This tool is able to compute satisfactorily the post-cracking cyclic response of RC walls, in terms of global force-displacement as well as the displacement at which concrete softening initiates or concrete crushes. The model represents well the flexure-shear interaction typically observed in squatter walls. Moreover the model accounts for mesh size effects. The model is also able to compute satisfactorily the cyclic response of walls with openings coupled through beams that remain elastic.

LITERATURE REVIEW

Modeling approaches for RC walls may be divided in five main categories: i) lumped plasticity models; ii) truss or strut and tie models; iii) macro-models like the stringer and panel model; iv) fiber element models; and v) finite element (FE) models. The simplest of the modeling approaches lumps all plasticity in a single location.[6-8] In lumped plasticity models flexure-shear interaction has been implemented by empirical calibration of nonlinear hysteretic rules. Truss models[9-17] have been used to evaluate the linear and nonlinear behavior of RC structures and members subjected to monotonic or cyclic loading. Some of these models[13,15,17] have been used to compute the nonlinear dynamic response of RC columns and walls. Design codes, such as

ACI[18] and CEB-FIP[19] have also adopted strut-and-tie models for the assessment[18] and design[18,19] of RC members. Stringer and panel model[20] uses nonlinear stringers that carry the shear flow and nonlinear panels to represent reinforced concrete panels. Fiber element models use multiple vertical elements to model concrete and reinforcing steel. Fiber element models for RC walls were first proposed in the 1970s.[21-23] Variations of these models have been used repeatedly.[24-33] Some of these models represent flexure-shear interaction through the use of nonlinear shear springs or through kinematic assumptions and constitutive laws at the section level, which are calibrated with experimental work. Fiber models[27,33] that model the transverse steel reinforcement and represent FSI using equilibrium, specific assumptions for the shear strain field, and bi-axial concrete material laws have also been developed. Modeling of RC walls using FE techniques is often complex, requiring much computational effort. Nonlinear finite element methods that use smeared and/or discreet crack approaches as well as plasticity models are well known,[34-47] but these methods have their own limitations and are used mainly by specialized consultants and in academia.

NONLINEAR TRUSS MODELING APPROACH

Truss Elements

Figure 1(a) shows a cantilever wall of length L_w and story height h. Its geometry and reinforcement are depicted in Fig. 1(b). Figure 1(c) shows a truss model for the wall panel with parallel angle diagonal elements. The layout of diagonal truss elements resembles, but does not need to match, the principal compressive stress trajectories when approaching the ultimate load, see Fig 1(d). The diagonal truss elements represent concrete only. The cross-section area of a diagonal truss is the product of the effective width b_{eff} and the width b_w of the wall. The effective

width b_{eff} depends on the lengths a and b of the subpanel, see Fig. 1(d) and thus on the angle θ_d of the diagonals. When the wall width varies, the width of the truss element is that of the wall at the locations of the element. The model also has horizontal and vertical truss elements. These truss elements represent reinforcing bars and their surrounding concrete. Effective areas of concrete and reinforcing bars are used, in the horizontal and vertical direction, as shown in Fig. 1. The position of the outer vertical elements, with a distance D between them as shown in see Fig. 1(c), is determined based on the position of the longitudinal reinforcement close to the wall's ends.

For each panel like this shown in Fig. 1(b), a minimum number of 4 subpanels is proposed to have an acceptable distribution of the vertical, horizontal effective areas of steel and concrete. In this study the minimum number of subpanels used was nine, see case studies 2, and 4 below. The proposed model better represents walls which develop a parallel diagonal compressive stress field. This can be the case of squat walls with significant flexure-shear interaction. A variable angle truss model[15-17] may better represent the fanned concrete compression stress field seen in slender and flexurally dominated walls.

In cases where walls and floor slabs frame, see Fig. 1, frame elements representing the mechanical properties of the slab over an effective width are used. For these elements, the area of reinforced concrete and reinforcing bars as well as the flexural rigidity of the effective slab width are used. The vertical, the horizontal, and diagonal truss elements and the frame elements are interconnected at nodes, see Fig. 1. Perfect bond between concrete and reinforcing steel is assumed. The model, as presented in this report, does not capture bond-slip and strain

penetration of anchored reinforcing bars, which can be an important flexibility source in flexural dominated members[48] not investigated here. If the constitutive stress-strain relationships of concrete and reinforcing steel are known, the truss' axial force - axial displacement relationship can be readily computed.

Truss Element Size Effect

It is well known that the prediction of the nonlinear response of a softening (strength degrading) structural element is very dependent of the mesh size in finite element modeling.[36,37,42] This computational mechanics problem is addressed by making the softening branch of the stress-strain relationships of the materials a function of the size of the elements used in the model. To account for the element size effect in this model, the notion of concrete fracture energy is employed.[36,37,42] Figure 2(a) shows a concrete panel of length L subjected to pure tension. Figure 2(b) depicts the assumed concrete axial stress f_c - crack opening u diagram of this element. The area under the f_c - u diagram is the fracture energy G_f. Figure 2(c) shows the f_c – strain ε relationship of the concrete element where ε is the result of smearing the crack opening u over the element length L. The area under the f_c - ε diagram is equal to G_f / L. Since G_f is a material property independent of L the f_c - ε relationship is adjusted according to the element length L. Increasing L results in a f_c - ε relationship with steeper degrading branch. The truss model described here considers the element size effect to determine the stress-strain behavior of concrete elements both in tension and compression as described below. In this study L is the length of a truss element in the model. As discussed below the element size effect also needs to be accounted for when determining the instantaneous compressive stress in a concrete truss element subjected to normal tensile strain.

Constitutive Stress-Strain Relationships

a. Reinforcing Steel - Vertical and Horizontal Truss Elements

The stress-strain relationship of steel is represented by the Dodd-Restrepo[49] hysteretic rule, see Fig. 3(a), where E_s is the initial modulus of elasticity, f_y the yield strength, f_{su} the ultimate stress that occurs at strain ε_{su}. The strain at initiation of strain hardening region is denoted as ε_{sh}. The model is described in detail by Dodd and Restrepo.[49] This model represents the Bauschinger effect and the degradation in the unloading modulus observed experimentally.[49] This model does not represent of the nonlinear geometrical response of a reinforcing bar (bar buckling). In addition to E_s, f_y, f_{su}, ε_{su}, ε_{sh}, the model requires as an input the parameter Ω which controls the shape of the stress-strain relationship in terms of Bauschinger effect. [49] In this report Ω = 0.9 was considered for all case studies described below.

b. Concrete Type I – Vertical and Horizontal Truss Elements

Concrete type I is used to model the vertical and horizontal concrete truss elements. These elements model the effective concrete area and account for tension stiffening.[5] The hysteretic stress-strain behavior of Concrete Type I, both in tension and compression, is modeled using the Schoettler - Restrepo's[50] piecewise linear rule shown in Fig. 3(b). For concrete in tension, the modulus of elasticity is $E_c = 2f_c'/\varepsilon_o$, where f_c' is the strength in MPa (1 ksi = 6.89 MPa), and ε_o = 0.2% is the strain of the unconfined concrete at f_c'. The direct tensile strength of concrete in MPa (1 ksi = 6.89 MPa) is $f_{ct} = 0.33\sqrt{f_c'}$, while the residual strength of concrete in tension is $f_{t,res}$ = $0.2f_{ct}$ at a strain $\varepsilon_{res} = 8\varepsilon_{cr}$ where ε_{cr} is the cracking strain of concrete. The values of $f_{t,res}$ and ε_{res} can be taken as a variable to account for the dependence of the average tension stiffening behavior to reinforcing steel ratio and bond conditions.[51]

The concrete stress-strain relationship used in this study unloads from tension with E_c until reaching a zero stress and then reloads to a compressive stress equal to f_{ct} at a compressive strain equal to ε_{cr}. The concrete compressive stress-strain relationship is assumed linear initially up to $f_c = 0.3\beta f_c'$ and characterized by a modulus of elasticity E_c. Factor β describes the dependency of the concrete compressive stress-strain relationship to the normal tensile strain as will be explained in the other concrete type model. In Concrete Type I, $\beta = 1$. Degradation occurs upon reaching $\beta f_c'$ and the concrete looses all its compressive strength at a strain ε_u. In the modified compression field theory[5] (MCFT), a recommended value is $\varepsilon_u = 0.4\%$. In the MCFT strains were measured and averaged over a region of 0.6 m (23.6 in.) by 0.6 m. (23.6 in.). Having as a reference the MCFT accounting for mesh size effects makes ε_u a function of element length L with ε_u = 0.6 x 0.4% = 0.24% / L, where L in meters (1 m = 23.6 in.). To avoid a very abrupt softening branch for panels larger than those reported in MCFT, ε_u = max (0.24% / L, 0.4%) is proposed in this study. The confined concrete in compression is assumed to yield but not to harden after reaching the confined compressive strength f_{cc} at a strain ε_{cc}, see Fig. 3(b). Confined concrete starts to degrade at strain ε_{cu}. Confined concrete values of f_{cc}, ε_{cc} and ε_{cu} are computed in this study based on the recommendations of Mander et al.[52] The concrete stress-strain relationship used in this study unloads with a modulus E_{cu}, reduced in comparison with E_c, until reaching a zero stress, see Fig. 3(b). The stress continues to be zero until the strain becomes zero and reloading in tension initiates.

c. Concrete Type II - Diagonal Truss Elements

Concrete Type II is used to model the diagonal concrete truss elements. More complex in response than the Concrete Type I, this model couples the element's compressive stress-strain

behavior to the tensile strain normal to the element's axis, ε_{t1}. This tensile strain is computed at the element's mid-length, see Fig. 4(a). For the truss element extending from nodes A to B, the instantaneous compressive stress is multiplied by factor β determined from the instantaneous tensile strain normal to the axis of the truss element. The tensile strain normal to the axis of the element is defined as the average strain computed with the zero stiffness "strain gage" elements OC and OD, see Fig. 4(a). The gage elements OC and OD are not necessary to coincide with truss elements used in the model. In this study the gage elements were coinciding with the truss elements of each subpanel. The angle formed between the elements AO and OD is denoted as θ_g, see Fig. 4(a). In this study $84^o < \theta_g < 106^o$ was used for the critical elements. Values of θ_g close to 90^o are recommended. Factor β is defined by the tri-linear relationship shown in Fig. 4(b). The tri-linear relationship proposed for factor β is based on that proposed by Vecchio and Collins,[5] but is capped at a value of $\beta_{res} = 0.3$ at a strain $\varepsilon_{tres} = 1.0\%$. As it will be discussed later in the discussion, factor β needs to be also a function of the gage length L_g to ensure mesh objectivity. Mesh objectivity describes the independence of the computational results on the size of the elements comprising the computational model. The hysteretic stress-strain behavior of Concrete Type II is represented by the piecewise linear rule shown in Fig. 3(b). Concrete Type II in tension has zero tensile strength f_{tres} at the tensile strain ε_{res}. Accounting for the element length effect ε_{res} is a function of L with $\varepsilon_{res} = \max (1.2\varepsilon_{cr} / L, 2\varepsilon_{cr})$. A minimum value of $\varepsilon_{res} = 2\varepsilon_{cr}$ is considered to avoid very abrupt softening branches in case of elements of large length.

MODEL VALIDATION

The model proposed was coded into the nonlinear structural analysis computer program Ruaumoko.[50] Existing rules available from the library in this program were used to represent

Concrete Type I, II and reinforcing steel. The model is validated by comparing the computed and experimentally measured response of five RC walls that were tested under reversed cyclic loading conditions. The cyclic response was computed using a displacement control algorithm. The following sections describe in detail the five walls considered and present the comparison between the experimentally measured and the computed responses. The walls had a ratio M/VL_w varied between 0.45 and 2.9, where M is the bending moment in the wall and V is the applied lateral force at the top. Case studies one, two, four, and five were tested under controlled lateral displacements while the wall of case study three under controlled lateral force using a prescribed load protocol. The response of all the walls was characterized by crushing of the concrete carrying the diagonal compression stress field. For all case studies presented below, except case study 2, the experimentally measured response was plotted by digitizing the original plots. The loops obtained should only be regarded as a good approximation.

Case Study 1 - Sittipunt et al.[53] - Wall W2

Case study 1 is a squat wall with an aspect ratio M/VL_w = 1.4, see Fig. 5(a). The longitudinal reinforcement ratio in the boundary elements ρ_{lb} and the web ρ_{lw} was equal to 2.3 and 0.5%, respectively. In the transverse direction, this wall had a reinforcement ratio ρ_t = 0.8%. Values of f_c', as well as of f_y, f_{su}, ε_{sh} and ε_{su} of the the 16 mm (0.63 in.), 12 mm (0.47 in.), and 10 mm (0.39 in.), and 6mm (0.24 in.) diameter bars are listed in Fig. 5. Lateral forces were applied at the top beam. This beam remained free to rotate throughout the test. No axial load was applied to the wall in this test. After reaching the theoretical flexural strength, the wall failed by web crushing at a lateral displacement of 30 mm (1.18 in.) corresponding to a drift ratio Θ_r = 1.4%.[53]

Figure 5(b) shows two truss models for Wall W2: M1-1 and M1-2. The two outer vertical elements on each side of the model represent the areas of reinforcing steel and concrete of the boundary elements, while the vertical lines of elements in between represent the tributary area of reinforcing steel and concrete in the web. Model M1-1 uses two vertical lines of elements in the web while, M1-2 uses three lines. Figure 5 lists the areas of the concrete and steel truss elements A_c, A_s, respectively. The subscripts v, and h refer to the vertical and horizontal elements, respectively, while the subscripts w, and b, refer to the web and the boundary elements, respectively.

Figure 6(a) compares the lateral force–lateral displacement response measured during the test with the responses predicted monotonically and cyclically using the M1-1 model. The response computed with model M1-2 is discussed in a following section. Model M1-1 computes well the cyclic response in terms of strength, loading and unloading stiffness. The displacement amplitudes at which softening initiation and crushing of the concrete diagonals is computed for first time are also indicated in this figure. The computed strength is 5% less than the experimentally measured for positive displacement response. In good agreement with the test response model M1-1 computes initiation of compression softening and crushing of concrete diagonals at Θ_r = 1.3%, and 2.5%, respectively.

Figure 7 compare the experimentally measured, using strain gauges, and computed longitudinal and transverse strains, respectively, versus lateral force. The points where strains are measured and computed are shown in Figure 5. The model satisfactory computes both the longitudinal and

transverse strains. The computed strains are smeared over the length of the element, while the experimentally measured strains, using strain gauges, are affected by bond slip, crack opening and strain localization.

Case Study 2 – Massone[54] – Wall WP1105-8

Case study 2 is a very squat wall with an aspect ratio M/VL_w = 0.45, see Fig. 8(a). The wall was lightly reinforced in the longitudinal and transverse directions. The wall longitudinal and transverse reinforcement ratios were ρ_{lw} = 0.43% and ρ_t = 0.27%, respectively. As in previous units, lateral force was applied to the wall via a top beam. In this test, the top beam was constrained from rotating, resulting in a point of inflection at the wall mid-height. The compressive axial load ratio was $N / f_c' A_g$ = 0.05 and remained constant during the test. Diagonal crushing of the concrete and loss of gravity load resistance was observed at Θ_r = 0.8%,[54] before the wall reaching its flexural strength.

Figure 8(b) shows two models: M2-1 and M2-2. Model M2-2 has elements with half the length of model's M2-1 elements. Figure 8 lists the areas of A_s and A_c used for the two models. The subscripts 1 and 2 refer to the outer and inner vertical elements, respectively. Figure 6(b) compares the measured and the computed response with the M2-1 model. The computed response with model M2-2 is discussed in a following section. Model M2-1 computes larger precracked stiffness. This is expected especially for this case where the wall is lightly reinforced in both directions and the effect of concrete in tension is important in both of them. Very satisfactory is the computed the point where the sudden drop in the force was observed at Θ_r = 0.84%. The model computes that the first diagonal reached ε_o in compression at Θ_r = 0.72%

while all of its compressive strength was lost at Θ_r = 0.86%. The computed lateral force exceeded the experimentally measured by by 10%.

Case Study 3 – Shiu et al.[55] – Perforated Wall PW1

Case study 3 is a moderately slender wall with an aspect ratio M/VL_w = 2.9. This is a six-story RC wall with openings built at 1:3 scale, see Fig 9(a). Lateral force was applied at the top of the wall. The test set up for this wall allowed its top end to rotate freely. The longitudinal portion of the wall was heavily reinforced with reinforcement ratios in the boundary elements and web equal to ρ_{lb} = 5.6 % and ρ_{lw} = 0.3%, respectively. The transverse reinforcement ratio was ρ_t = 0.4%. The longitudinal and transverse steel ratio of the coupling beams were ρ_{ll} = 0.7%, and ρ_{tb} = 0.9%, respectively. These beams were designed to and remained elastic during the test.[55] Figure 9(b) lists the f_y, f_{su}, ε_{sh}, ε_{su}, of the #3, #4 and 6 mm (0.24 in.) bars, respectively, employed in this test. Diagonal compression failure of the web, extending also in the boundary element, was observed at the first floor in the last cycle for negative displacement corresponding to Θ_r = 2.4%.

To model this structure, the longitudinal portion of the perforated wall was discretized in individual panels having an aspect ratio of h / L_w = 1.2, see Figs. 9(a) and 9(c), representing the part of the wall on the sides of the openings; additional wall panels between the openings of the two subsequent floors have an aspect ratio of h_2 / L_{w2} = 1.4. The panels are modeled as shown in Fig. 9(c). Figure 6(c) compares the measured and the computed response, M3, for the perforated wall. The model computes satisfactorily the overall cyclic response of the wall. The diagonal

concrete reaches ε_o at Θ_r = 1.4%, while it crushes at Θ_r = 1.7%. The computed peak lateral force is 6% smaller than the experimentally measured.

Case Study 4 – Massone[54] – Wall WP1111-9

This wall has identical dimensions, reinforcement details, and reinforcing steel properties with the wall of case study 2. The differences, in comparison with the wall of case study 2, are the axial load ratio which is equal to 10% and the $f_c^{'}$ = 28 MPa (4.1 ksi). For this specimen a wide diagonal crack, from corner to corner of the specimen, sliding along the crack, and onset of strength degradation was observed[54] at Θ_r = 0.6%.

Figure 10 compares the measured and computed response with the M2-1 model. The model, similar to case study 2, computes larger pre-cracked stiffness in comparison with the experimentally measured. Very satisfactory is the computation at the onset of strength degradation at Θ_r = 0.6%. The model computes that the first diagonal reached ε_o in compression at Θ_r = 0.53% while it crushed at Θ_r = 0.76%. The peak computed lateral force exceeded the experimentally measured by 9%.

Case Study 5 - Oesterle et al.[56] – Wall B9

Case study 5 is a moderately slender wall with an aspect ratio M/VL_w = 2.4, see Fig. 11(a). The wall had heavily reinforced boundary elements, with a longitudinal reinforcement ratio of ρ_{lb} = 3.7%. The wall web had longitudinal and transverse reinforcement ratios equal to ρ_{lw} = 0.3%, and ρ_t = 0.55%, respectively. The concrete compressive strength, $f_c^{'}$, the reinforcement yield strengths, f_{ylb}, f_{ylw}, f_{yt}, and f_{yc} of the longitudinal reinforcement in the boundary elements and the

web, of the transverse reinforcement and the confining reinforcement in the boundary elements, respectively, are listed in Fig.11. The test set up allowed this beam to rotate freely during the test. The compressive axial load ratio was $N / f_c' A_g$ = 0.09. First indication of crushing of the diagonals was noted for peak negative load,[56] after the wall had developed its theoretical flexural strength. Crushing of the concrete carrying the diagonal compression stress field in the wall occurred the first time the peak negative displacement, corresponding to Θ_r = 3.0%,[4] was reached.

Figure 11(b) shows the truss model, M5, for Wall B9. The outer vertical elements represent the areas of reinforcing steel and concrete of the boundary elements, while the three vertical lines of elements in between represent the area of reinforcing steel and concrete in the web.

Figure 12(a) compares the measured and computed lateral force-lateral displacement hysteretic response. The model computes satisfactory the cyclic response and the displacement at which crushing of the concrete in the diagonals occurred is observed. The computed response demonstrates more pinching. The computed peak lateral force exceeded the experimentally measured by 3%.

DISCUSSION

The previous section showed that the truss model described in this report can compute with a reasonable level of accuracy the cyclic response of RC walls, of different geometries whose response is largely affected by flexure-shear interaction. As expected, the model computes larger uncracked stiffness because of the overlapping of the cross-section areas in the horizontal,

vertical and diagonal concrete truss elements. This should be considered if the model is used to compute the dynamic response of RC wall buildings under low- or moderate-intensity earthquake excitations and especially when the wall is lightly reinforced. Nevertheless, upon cracking, the theoretical and experimental stiffness compares well. Table 1 lists the ratio of computed to measured secant stiffness $r_{K,s,0.7,Fu,m}$ at lateral force equal to 0.7 of the peak measured lateral force $F_{u,m}$. In all cases the computed secant stiffness doesn't exceed the measured by more than 19% with the average overestimation of the secant stiffness to be 16%.

Furthermore, the model reasonably computes the lateral force and displacement at which the concrete carrying the compression stress field crushes in a wall. This is because the model: i) appropriately computes the cyclic strain history of the elements, ii) updates the stress-strain relationship of concrete (Concrete Type II) according to the instantaneous normal tensile strain in each of the diagonal truss elements carrying compression. However, such computations are sensitive on the element size chosen in the model. Suitable modifications to the softening part of the stress-strain relationships for concrete are needed to account for the element size effect to address the strain localization problem. In subsection *Truss Element Size Effect*, the authors described a standard method used in computational mechanics to address this problem. In the following sections the authors discuss additional issues that need to be considered to address the strain localization phenomena and ensure mesh objectivity.

Mesh Objectivity

Figures 13(a) to 13(c) compare the lateral force-displacement responses computed for wall WP1105-8, examined previously in case study 2, using the model M2-1 and three variants of

model M2-2, see Fig. 8(b). Each variant of model M2-2 has a different stress-strain relationship for concrete. The first variant of model M2-2, M2-2-1 the stress-strain relationship for concrete is made a function of the element length, as discussed in section *Concrete Type II - Diagonal Truss Elements***.** This model uses the same relationship for β as in model PA-43. Figure 13(a) shows that model M2-2-1 results in a significantly different overall force-displacement response, in comparison with M2-1, with 20% smaller peak lateral force. Model M2-2-1 displays much earlier softening of the concrete diagonals than model M2-1.

Fig. 14 shows the computed normal tensile strain histories for elements e_1 and e_2, which are the upper left diagonal truss elements of models M2-1 and M2-2-1, respectively, see Fig. 8. In these elements first the concrete crushes. Figure 14 shows that the normal tensile strain computed for element e_2 in model M2-2-1 is on average twice the normal tensile strain obtained for element e_1 in model M2-1. The increased tensile strain in element e_2 is due to strain localization in tension in this element. The larger normal tensile strain of this element results in earlier reduction of factor β in model M2-2-1 when compared to model M2-1, see Figure 14 (b). This explains why the response computed by model M2-2-1 softens at a smaller drift than that computed by model M2-1. This comparison demonstrates that the modification of the stress-strain relationship of concrete alone, as examined in Section *Concrete Type II - Diagonal Trusses* is not sufficient to solve the element size conundrum in these models.

A key in the solution of the element size problem is the recognition that the strain localization phenomena also exists in the diagonal strain gauge elements, which monitor the normal tensile strain in a diagonal truss element in compression via factor β. For example, compare the

response predicted by model M2-2-2, the second variant of model M2-2, with the response computed by model M2-1. Model M2-2-2 makes the stress-strain relationship for concrete a function of the element length and also makes the tensile strain $\varepsilon_{tres,}$ a linear function of the element length. Since the length of the elements in model M2-2 are half those of M2-1, we intuitively make ε_{tres} = 2.0% in model M2-2-2, which is 2 times the value used in M2-1. Figure 13(b) shows that model M2-2-2 significantly improves the computed response for drift ratio up to 0.7%. When ε_{tres} = 3.5%, as is incorporated into the third variant of model M2-2, model M2-2-3, the responses predicted by this model and the coarser mesh model M2-1 practically overlap, see Fig. 13(c).

Relationship between Factor β and Transverse Element Gage Length

The comparisons made in previous section showed the significant effect that the element size has on the computed response, when this involves softening. Models M2-2-1 and M2-2-2 showed that the softening branch of the stress-strain relationship for concrete and that the relationship defining factor β for concrete should be made a function of the element length. However, there are few cases where mesh objectivity cannot be attained fully. One such case is when strain localization occurs in a diagonal truss element in compression and in a strain gauge element that it is not connected to the compressive element that experienced localization.

The element length invariant relationship for factor β shown in Fig. 4 with ε_{tres} = 1.0% is a simple representation of the nonlinear relationship proposed by Vecchio and Collins.[5] Such relationship was based on results of shear panels that had a reference gauge length L_{gR} = 0.6 m (23.6 in.) equal to the length over which smeared strains were measured, for which the residual strain was set ε_{tres} = 1.0%. Hence, an element length dependent residual strain can be defined as:

$$\varepsilon_{tres} = 1.0\% \times \left(\frac{L_{gR}}{L_g sin\theta_g} \right) = \frac{0.6\%}{L_g sin\theta_g} \tag{1}$$

where L_g in meters. This relation of β and L_g implies that localization in tension and compression will occur in the same subpanel. The ratio of $L_{gR} \Big/ \left(L_g sin\theta_g \right)$ of the diagonal elements of the web parts of the models of case studies one to five is equal to 1.3, 1.1, 2.1, 1.1, and 1.3, respectively. Assuming a relation of β which depends on the gage length L_g the response of case study three is recomputed. Figures 15(a) shows the comparison of the computed response for case study three using the newly defined relationship for β. The computed responses, with (M3g) and without (M3) considering the effect of gage length on β, are compared in this plot. As expected model M3g computes at a later stage strain ε_o in compression and crushing in the concrete diagonals. For both sides of displacement response model M3g results in larger peak lateral force. The computed response using model M3g is closer to the measured, compare Figures 6(c) and 15(a). Similarly for case study 5 accounting for mesh size effects in the biaxial behavior of concrete (model M5g) results in computation of first softening and crushing of the diagonals at a later stage, compare Figures 12(a) and 12(b). In this case accounting for the mesh size effects in the biaxial behavior of concrete results in better agreement between measured and computed response.

Angle of Inclination of Diagonal Truss Elements

Figure 15(b) compares the response of models M1-1g and M1-2g of case study one. For both models factor β is a function of the gage length. Model M1-2g with steeper angles computes softening and crushing of the concrete diagonals for a smaller drift ratio, in comparison with M1-

1g. Model M1-2g results in more strength degradation for both sides of the response, and especially for negative displacement corresponding to drift ratio larger than 1.0%. The sensitivity of the computed response on the angle of the diagonal struts has been also indicated by Mazars et al.[13].

CONCLUSIONS

This report described a nonlinear truss modeling approach for reinforced concrete walls. Longitudinal, transverse, and diagonal truss elements were used to represent concrete and reinforcing steel. The model represents well flexure-shear interaction by appropriately computing the strains in the reinforcement and in the concrete and by updating the concrete compressive stress-strain relationship with the instantaneous tensile strain normal to the diagonal elements carrying the compression stress field. The model accounts for the element length effects to determine the concrete stress-strain relationship. The model was verified by comparing the computed and experimentally measured response of five RC walls with response characterized by significant flexure-shear interaction including a wall with openings. Parallel angle truss model with diagonals, in the web part of the walls, of length between 0.3m and 0.5m and angles between 43^o and 53^o were used to model panels with M/VL_w ratios between 0.45 and 2.9. The main conclusions drawn are:

1. The nonlinear cyclic truss model computes reasonably well the post-cracking cyclic force-displacement response of RC walls, with significant flexure-shear interaction in their response, in terms of strength and stiffness, with moderate computational effort. The model computes larger, than the experimentally measured, pre-cracked stiffness due to the overlapping areas of vertical, horizontal and diagonal concrete elements. The computed

secant stiffness at 0.7 of the peak measured force was found to be 16% larger, on average, than the experimentally measured one.

2. Accounting for the element length effects is important for the computation of the overall force-displacement response and especially for the computation of the local element response involving softening.
3. In the case study where mesh objectivity was investigated, this required consideration of the effects of element length not only in the determination of the uniaxial stress-strain behavior of concrete but also to determine the relation between the concrete compressive stress-strain behavior and normal tensile strain.
4. For the one case where the effect of angle of the diagonals investigated, steeper angles resulted in earlier crushing of the diagonals and more strength degradation.
5. Using a panel discretization approach, a truss model can be effectively used to predict the cyclic response of walls with openings coupled through beams that remain elastic.

ACKNOWLEDGEMENTS

We would like to thank the Portland Cement Association (PCA) which partially supported the first author for this work, and Professor Athol Carr for his insightful comments.

REFERENCES

1. FEMA. NEHRP Guidelines for the Seismic Rehabilitation of Buildings, FEMA 273, and NEHRP Commentary on the Guidelines for the Seismic Rehabilitation of Buildings, *FEMA 274*. Federal Emergency Management Agency, Washington, D.C., 1997, 435 pp.

2. FEMA. Prestandard and Commentary for the Seismic Rehabilitation of Buildings, *FEMA 356*. Federal Emergency Management Agency, Washington, D.C., 2000, 519 pp.
3. Pujol, S., Sozen M. and Ramirez, J, "Transverse Reinforcement for Columns of RC Frames to Resist Earthquakes," *J. Struct. Eng.*, V. 126, 2000, pp. 461-466.
4. Oesterle, R. G., Fiorato, A. E., Johal, L. S., Carpenter, L. S., Russell, H. G., and Corley, W. G., "Earthquake-Resistant Structural Walls - Tests of Isolated Walls," Report to the National Science Foundation , Construction Technology Laboratories, Portland Cement Association, Skokie, Illinois, 1976, 315 pp.
5. Vecchio, F. J., Collins, M., P., "The Modified Compression Field Theory for Reinforced Concrete Elements Subjected to Shear," *Journal of the American Concrete Institute*, V. 83, No. 2, 1986, pp. 219-231.
6. Giberson MF. Two Nonlinear Beams with Definitions of Ductility. Journal of the Structural Division ASCE, 1969, pp. 137-157.
7. Saiidi M., Sozen M. A, "Simple and Complex Models for Nonlinear Seismic Response of Reinforced Concrete Structures," Structural Research Series No. 465. University of Illinois, Urbana (Illinois), USA, 1979, 204 pp.
8. Hidalgo, P. A., Jordan, R. M., and Martinez, M. P., "An Analytical Model to Predict the Inelastic Seismic Behavior of Shear-Wall, Reinforced Concrete Structures," *Engineering Structures*, V. 24, No. 1, 2002, pp. 85-98.
9. Hrennikoff, A. "Solution of Problems of Elasticity by the Framework Method," *Journal of Applied Mechanics*, (Trans ASME), 1941, pp. 169-175.
10. Absi, E., Prager, W., "A Comparison of Equivalence and Finite Element Methods," Computer Methods in Applied Mechanics and Engineering, V. 6, No. 1, 1975, pp. 59-64.
11. Schlaich, J., Schaefer, K. and Mattias, M., "Toward a Consistent Design of Structural Concrete," Special Report of PCI Journal, V. 32, No. 3, 1987, pp. 75-150.

12. Tjhin, T. N., and Kuchma, D. A. "Computer-Based Tools for Design by Strut-and-Tie Method: Advances and Challenges," *ACI Structural Journal*, V. 99, No. 5, 2002, pp. 586-594.
13. Mazars, J., Kotronis P., and Davenne, L. "A new Modelling Strategy for the Behavior of Shear Walls Under Dynamic Loading," *Earthquake Engineering and Structural Dynamics,* V. 31, No. 4, 2002, pp. 937-954.
14. To, N. H. T., Ingham, J. M., Davidson, B. J., and Sritharan S., "Cyclic Strut-and-tie Modeling of Reinforced Concrete Structures," *Pacific Conf. on Earthquake Engineering*, Paper No. 102, Christchurch, New Zealand, 2003, 9 pp.
15. Miki, T., "Nonlinear Analysis of Reinforced Concrete Structures Subjected to Seismic Loads by Using Three-dimensional Lattice Model," *Ph.D. thesis*, Department of Civil Engineering, Tokyo Institute of Technology, 2004, 210 pp.
16. Park, H., and Eom, T, "Truss Model for Nonlinear Analysis of RC Members Subject to Cyclic Loading," *J. Struct. Eng.*, V. 133, No. 10, 2007, pp. 1351-1363.
17. Panagiotou, M., "Seismic Design, Testing and Analysis of Reinforced Concrete Wall Buildings," *Ph.D. Thesis*, Department of Structural Engineering, University of California, San Diego, 2008, 288 pp.
18. American Concrete Institute (ACI), "Building Code Requirements for Structural Concrete," *ACI 318-08*, Farmington Hills, Mich, 2008, 467 pp.
19. Comité Euro-International du Béton/Fédération Internationale de la Précontrainte. CEB-FIP model code 1990: Design code, *Thomas Telford*, London, 1993, 437 pp.
20. Blaauwendraad, J., and Hoogenboom P. C. J. "Stringer Panel Model for Structural Concrete Design*," ACI Structural Journal*, V. 93, No. 3, 1996, pp. 1-11.

21. Taylor, R.G. “The Nonlinear Seismic Response of Tall Shear Wall Structures”. Ph.D. Thesis, Department of Civil Engineering, University of Canterbury, 1977, 207 pp.
22. Otani, S. Kabeyasawa, T., Shiohara, H., and Aoyama, H., "Analysis of the Full Scale Seven Story Reinforced Concrete Test Structure," ACI SP-84, American Concrete Institute, 1985, pp. 203-239.
23. Vulcano, A., Bertero, V. V., “Analytical Models for Predicting the Lateral Response of RC Shear Walls: Evaluation of their Reliability,” *Earthquake Engineering Research Center*, University of California, Berkeley, 1987, 93 pp.
24. Fischinger, M., Vidic, T., and Fajfar, P., “Nonlinear Seismic Analysis of Structural Walls using the Multiple-vertical-line-element Model,” *Nonlinear Seismic Analysis and Design of Reinforced Concrete Buildings*. Fajfar, P., Krawinkler, H., editors. Elsevier Applied Science, 1992, 307 pp.
25. Linde, P., Bachmann, H., “Dynamic Modeling and Design of Earthquake-resistant Walls,” *Earthquake Eng. Struct. Dynamics*, V. 23, No. 12, 1994, pp. 1331-1350.
26. Ranzo, G., and Petrangeli, M., “A Fibre Finite Beam Element with Section Shear Modelling for Seismic Analysis of RC Structures”. *Journal of Earthquake Engineering*, V. 3, No. 2, 1998, pp. 443-471.
27. Petrangeli, M., Pinto, P. E., Campi, V., “Fiber Element for Cyclic Bending and Shear of RC Structures. I: Theory,” *Journal of Engineering Mechanics*, V. 125, No. 9, 1999, pp. 994-1001.
28. Petrangeli, M., “Fiber Element for Cyclic Bending and Shear of RC Structures. II: Verification,” *Journal of Engineering Mechanics*, V. 125, No. 9, 1999, pp. 1002-1009.

29. Ghobarah, A., Youssef, M. "Modelling of Reinforced Concrete Structural Walls," *Engineering Structures*, V. 21, No. 10, 1999, pp. 912-923.
30. Orakcal, K., Wallace, J. W., and Conte, J. P., "Nonlinear Modeling and Analysis of Slender Reinforced Concrete Walls," *ACI Structural Journal*, V. 101, No. 5, 2004, pp. 455-465.
31. Martinelli L. "Modeling Shear-Flexure Interaction in Reinforced Concrete Elements Subjected to Cyclic Lateral Loading," *ACI Structural Journal*, V. 105, No. 6, 2008, pp. 675-684.
32. Massone, L.M., Orakcal, K., Wallace, J. W., "Modeling of Squat Structural Walls Controlled by Shear," *ACI Structural Journal*, V. 106, No. 5, 2009, pp. 646-655.
33. Massone, L.M., Orakcal, K., and Wallace, J. W. (2006). "Shear - Flexure Interaction for Structural Walls," SP-236, *ACI Special Publication* – Deformation Capacity and Shear Strength of Reinforced Concrete Members Under Cyclic Loading, editors: Adolfo Matamoros & Kenneth Elwood, 127-150, 2006
34. Cervenka, V., and Gerstle, K. H., "Inelastic Analysis of Reinforced Concrete Panels: Theory," *Publ. IABSE*, V. 31, No. 11, 1971, pp. 31-45.
35. Vallenas, J. M., Bertero, V., and Popov, E. P., "Hysteresis Behavior of Reinforced Concrete Structural Walls," Report No. UCB/EERC-79/20, *Earthquake Engineering Research Center*, University of California, Berkeley, 1979, 267 pp.
36. Bazant Z.P., Ceolin L., 'Blunt Crack Propagation in Finite Element Analysis', *J. Eng. Mech. Div., ASCE*, V. 105, No. 2, 1979, pp. 297-315.
37. Pietruszczak, S. and Mroz, Z. "Finite Element analysis of deformation of strain softening materials," International Journal for Numerical Methods and in Engineering, V. 17, No. 3, 1981, pp. 327-334.

38. Balakrishnan, S., and Murray, D. W., "Prediction of R/C Panel and Deep Beam Behavior by NLFEA," *J. Struct. Engrg.*, V. 114, No. 10, 1988, pp. 2323-2342.

39. Crisfield, M. A., Wills J., "Analysis Of R/C Panels Using Different Concrete Models," *J. Engrg. Mech.* V. 115, No. 3, 1989, pp. 578-597.

40. Feenstra, P. H., de Borst, R., "Aspects of Robust Computational Modeling for Plain and Reinforced Concrete," Heron, V. 38, No. 4, 1993, 76 pp.

41. Park, H., Klingner, R.E., "Nonlinear Analysis of RC Members Using Plasticity with Multiple Failure Criteria," *J. Struct. Eng.*, V. 123, No. 5, 1997, pp. 643-651.

42. Bazant, Z. P., Planas, J., "Fracture and Size Effect in Concrete and Other Quasibrittle Materials". CRC Press, 1998, 616 pp.

43. Ayoub, A., Filippou F. C., "Nonlinear Finite-Element Analysis of RC Shear Panels and Walls," *J. Struct. Engrg.* 124, No. 3, 1998, pp. 298-308.

44. Palermo, D., Vecchio, F. J., "Behavior of Three-Dimensional Reinforced Concrete Shear Walls," *ACI Structural Journal*, V. 99, No. 1, 2002, pp. 81-89.

45. Mosalam, K. M., Mahin, S. A., and Rojansky, M., "Evaluation of Seismic Performance and Retrofit of Lightweight Reinforced Concrete Shear Walls," *ACI Structural Journal*, V. 100, No. 6, 2003, pp. 693-703.

46. Maekawa, K., Pimanmas, A., and Okamura H. "Nonlinear Mechanics of Reinforced Concrete," Spon Press. London, 2003, 721 pp.

47. Fédération internationale du béton (FIB). "Practitioners' Guide to Finite Element Modeling of Reinforced Concrete Structures." State-of-art report, Lausanne, Switzerland, June 2008, 344 pp.

48. Bertero, V. V., Popov, E. P., Viwathanatepa, S. “Bond of reinforcing steel: experiments and a mechanical model v. 2, Nonlinear behavior of reinforced concrete spatial structures,” *Contributions to the IASS Symposium*, 1978, pp. 3-17.

49. Restrepo-Posada, J. I., Dodd, L. L., Park, R., and Cooke N. “Variables Affecting Cyclic Behavior of Reinforcing Steel”, J. Struct. Engrg., V. 120, No. 11, 1994, pp. 3178-3196.

50. Carr, A. J., “Ruaumoko – A Program for Inelastic Time-History Analysis,” Department of Civil Engineering, University of Canterbury, New Zealand. 2008, 844 pp.

51. Bentz E. C., “Explaining the Riddle of Tension Stiffening Models for Shear Panel Experiments.” *J. Struct. Eng.*, V. 114, No 9, 2005, pp. 1422-1425.

52. Mander, J. B., Priestley, M. J. N., Park, R., “Theoretical Stress-Strain Model for Confined Concrete,” *J. Struct. Eng.*, V. 114, No. 8, 1988, pp. 1804-1826.

53. Sittipunt, C., Wood, S. L., Lukkunaprasit, P., Pattararattanakul, P. “Cyclic Behavior of Reinforced Concrete Structural Walls with Diagonal Web Reinforcement,” *ACI Structural Journal*, V. 98, No. 4, 2001, pp. 554-562.

54. Massone Sanchez L. M. “RC Wall Shear – Flexure Interaction: Analytical and Experimental Responses,” *Ph.D. thesis*, University of California, Los Angeles, 2006, 398 pp.

55. Shiu, K. N., Daniel, J. I., Aristizabal-Ochoa, J. D., Fiorato, A. E., and Corley, W. G., “Earthquake-Resistant Structural Walls—Tests of Walls With and Without Openings,” Report to the National Science Foundation, Construction Technology Laboratories, Portland Cement Association,Skokie, Illinois, 1981, 120 pp.

56. Oesterle, R. G., Fiorato, A. E., Johal, L. S., Carpenter, L. S., Russell, H. G., and Corley, W. G., “Earthquake-Resistant Structural Walls - Tests of Isolated Walls – Phase II,” Report to

the National Science Foundation , Construction Technology Laboratories, Portland Cement Association, Skokie, Illinois, 1979.

Table 1. Ratio of computed to measured secant stiffness at 70% of peak measured lateral force.

Case Study	1	2	3	4	5
$r_{K,s,0.7Fu,m}$	1.19	1.18	1.18	1.11	1.16

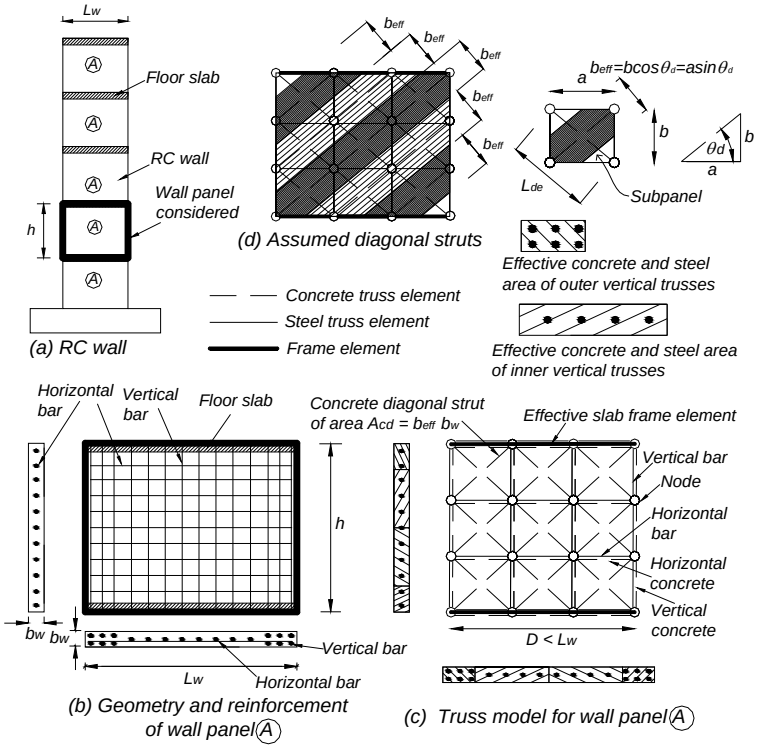

Figure 1. Reinforced concrete wall and wall panel truss model.

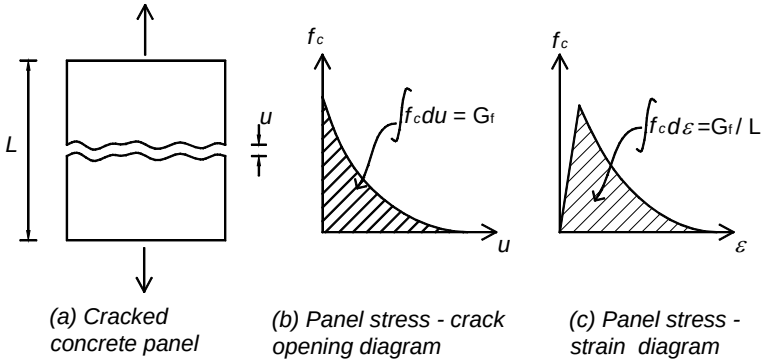

Figure 2. Tension softening behavior of a concrete element, (b) definition of fracture energy, and (c) relationship between stress-strain curve, fracture energy and element size effect.

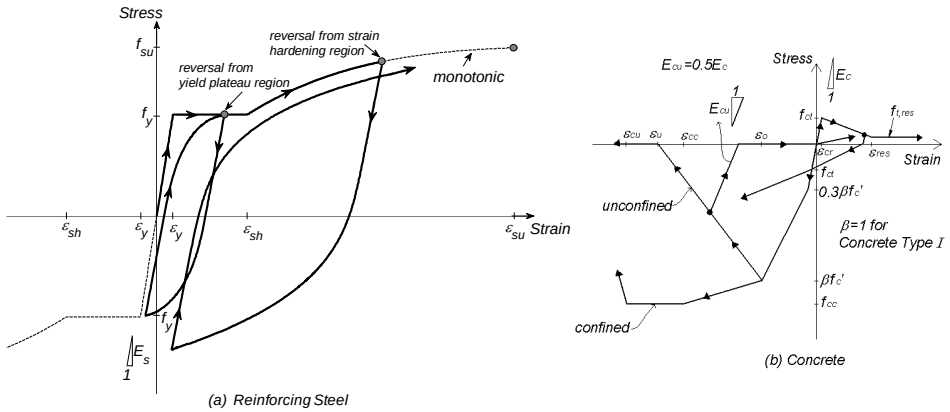

Figure 3. Stress-strain relationships of reinforcing steel and concrete.

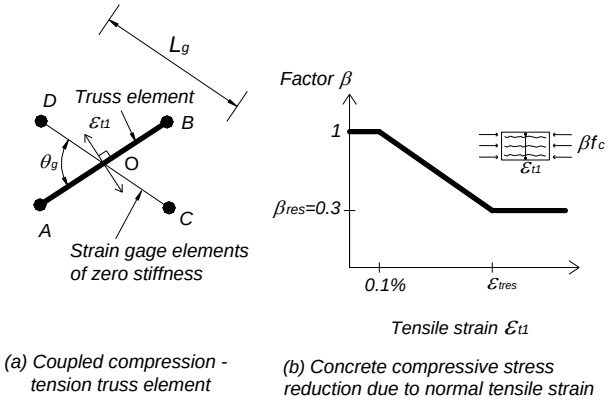

Figure 4. Coupled compression-tension model for diagonal truss elements.

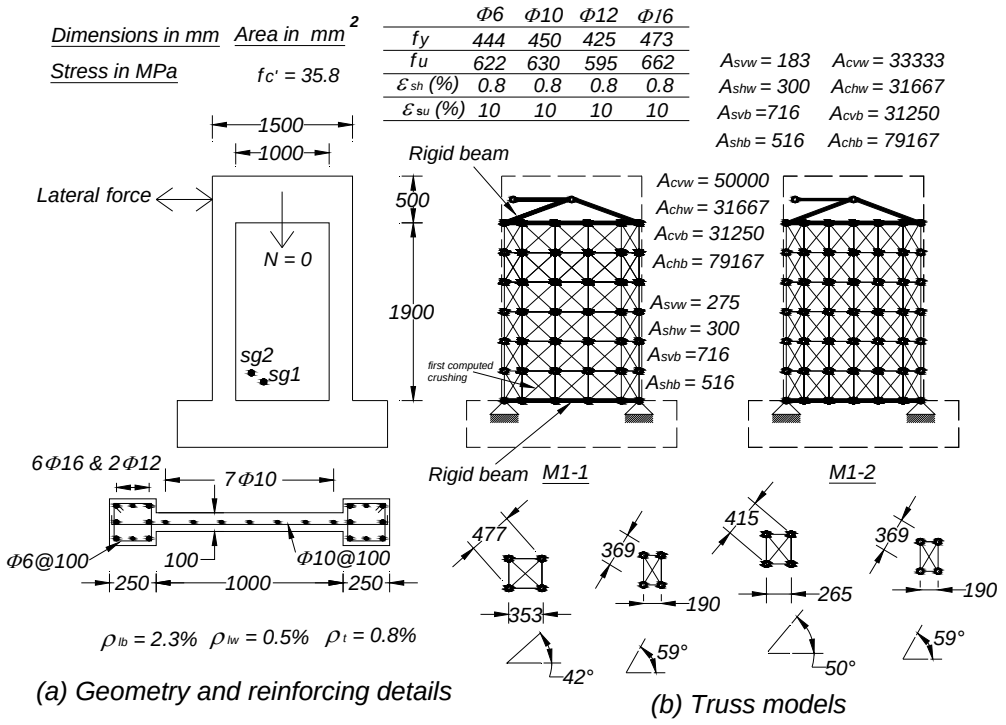

Figure 5. Study case 1 - Sittipunt et al.[53] - Wall W2. (25.4 mm = 1 in., 4.44 kN = 1 kip, 1MPa = 6.89 ksi).

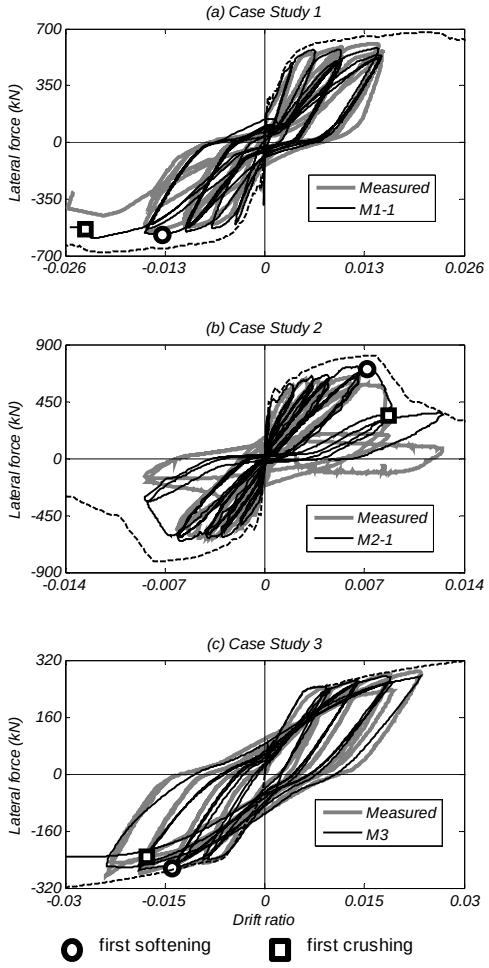

Figure 6. Comparison of experimentally measured and computed responses. Drift ratio computed at 2150 mm (84.6 in.) , 1219 mm (48 in.), and 5486 mm (216 in.) from base of wall specimens for case studies, 1, 2, and 3, respectively. (25.4 mm = 1 in., 4.44 kN = 1 kip, 1MPa = 6.89 ksi).

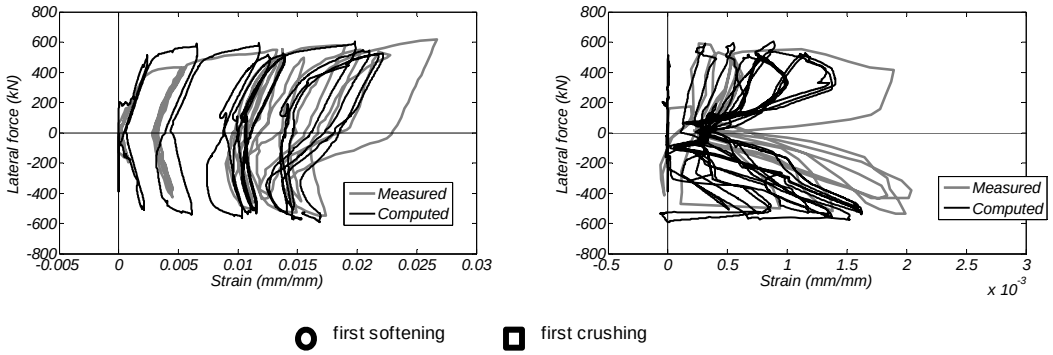

Figure 7. Case study 1 - Comparison of experimentally measured and computed strain versus lateral force: (Left) Longitudinal strain based on strain gauge 1 [sg1], (Right) Transverse strain using strain gauge 2 [sg2]. The location of sg1, and sg2 is shown in Figure 5 (25.4 mm = 1 in., 4.44 kN = 1 kip).

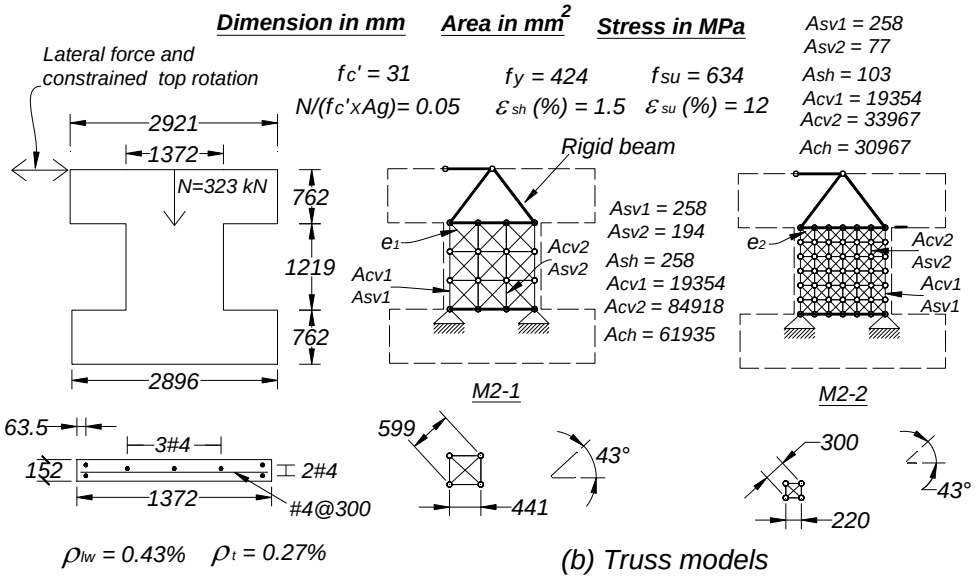

Figure 8. Case study 2 - Massone - Wall WP1105-8. (25.4 mm = 1 in., 4.44 kN = 1 kip, 1MPa = 6.89 ksi).

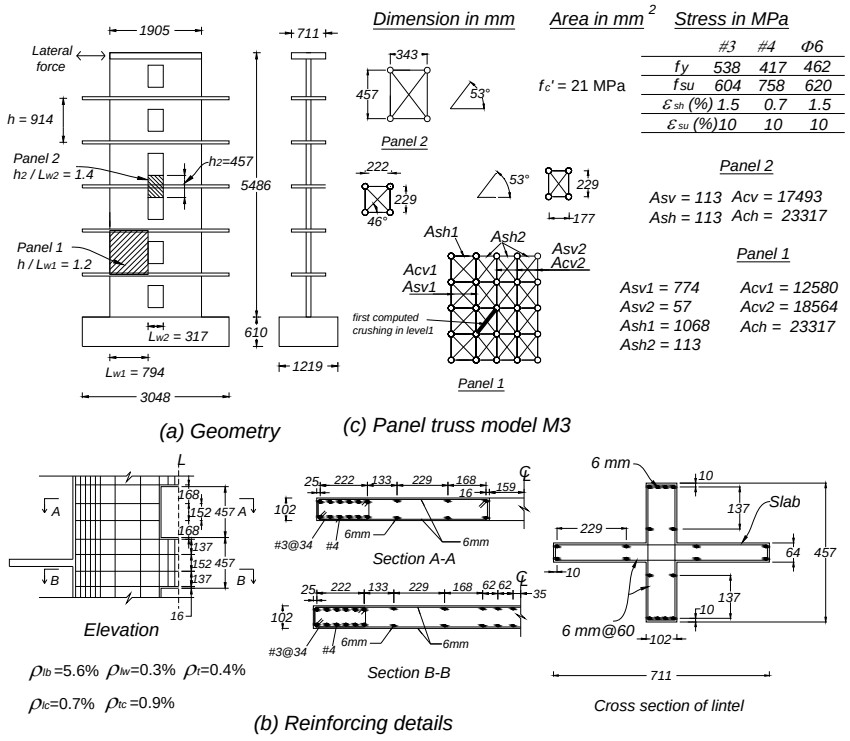

Figure 9. Case study 3 - Shiu et al. - Wall PW1. (25.4 mm = 1 in., 4.44 kN = 1 kip, 1MPa = 6.89 ksi).

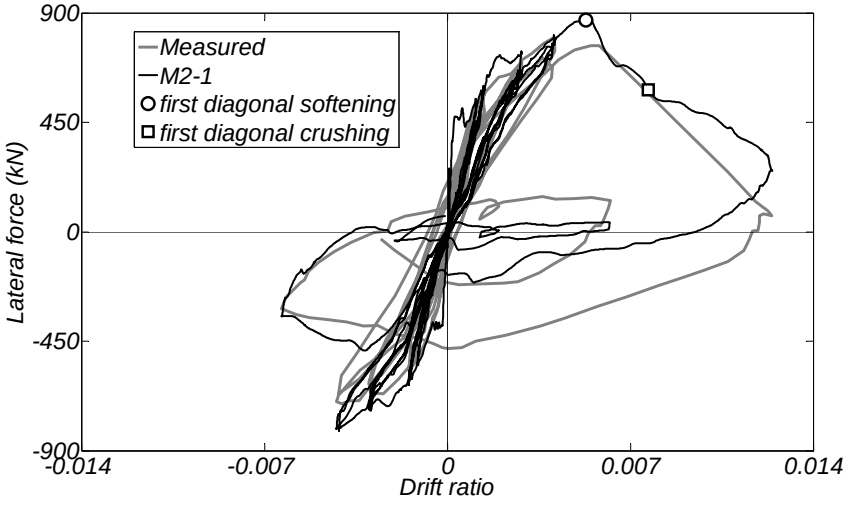

Figure 10. Comparison of experimentally measured and computed responses of case study 4 - Massone - Wall WP1111-9. (25.4 mm = 1 in., 4.44 kN = 1 kip, 1MPa = 6.89 ksi).

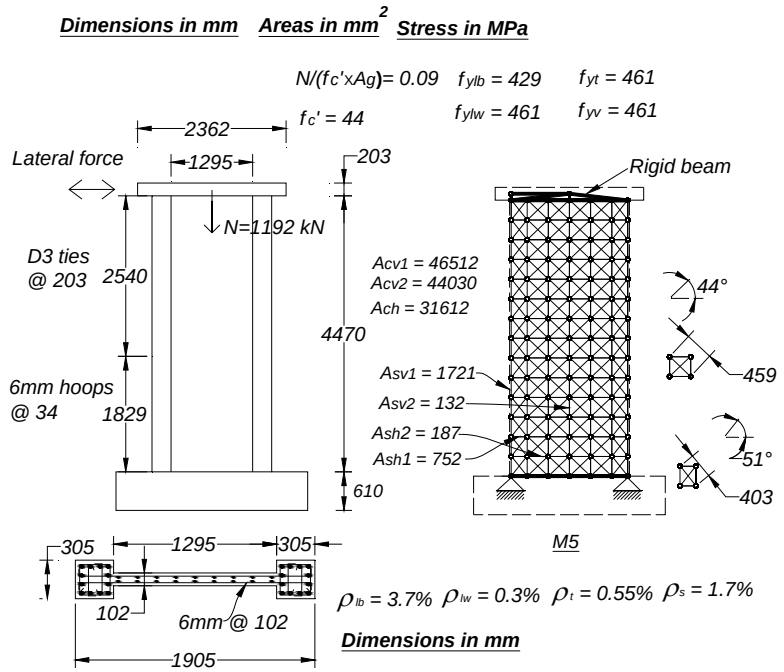

(a) Geometry and reinforcing details (b) Truss model

Figure 11. Case study 5 - Oesterle et al.[56] - Wall B9. (25.4 mm = 1 in., 4.44 kN = 1 kip, 1MPa = 6.89 ksi).

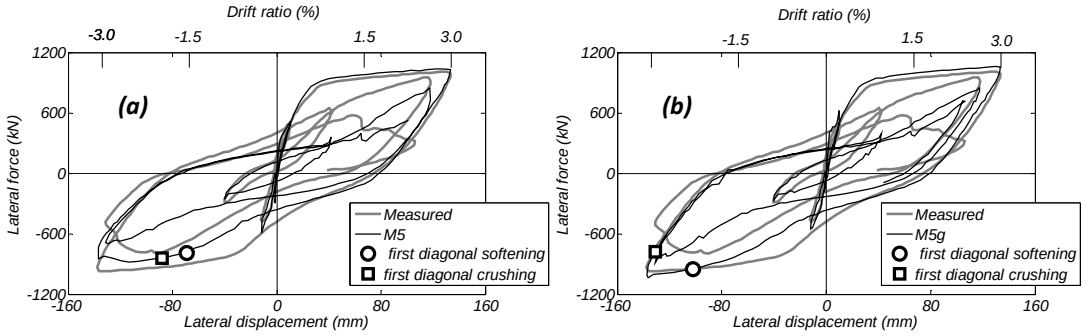

Figure 12. Comparison of experimentally measured and computed responses of case study 5 - Oesterle et al. - Wall B9. (25.4 mm = 1 in., 4.44 kN = 1 kip, 1MPa = 6.89 ksi).

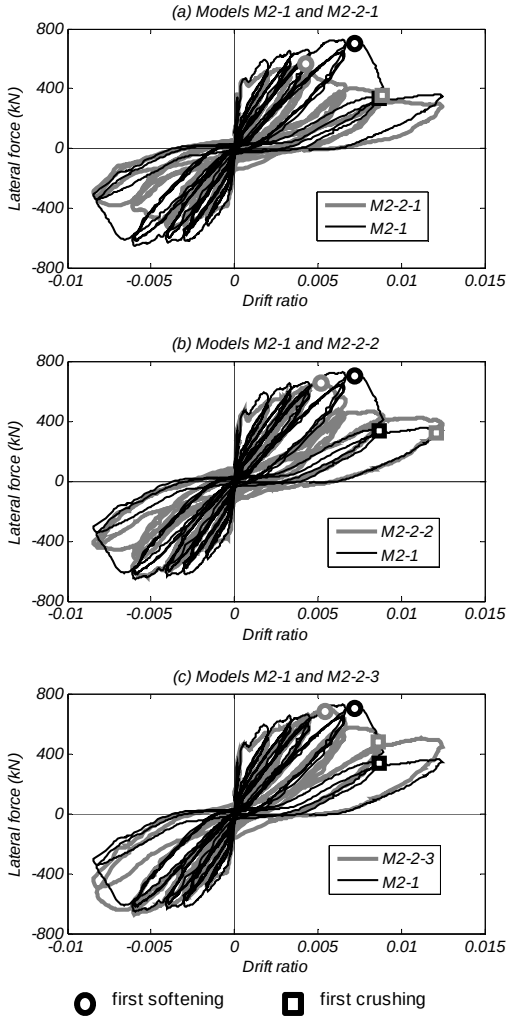

Figure 13. Mesh size effect for case study 2. Drift ratio computed at 1219 mm (48 in.) from base of wall specimen. (25.4 mm = 1 in., 4.44 kN = 1 kip, 1MPa = 6.89 ksi).

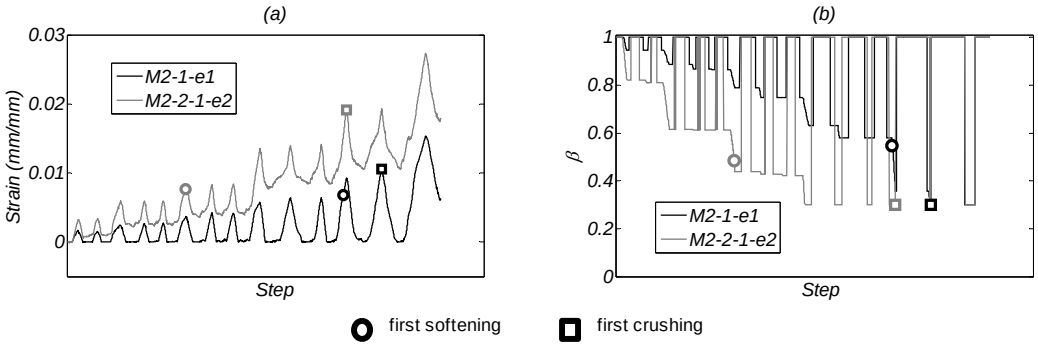

Figure 14. (a) Computed normal tensile strains and (b) Computed β factor of elements e_1 and e_2 of models M2-1 and M2-2, respectively. (25.4 mm = 1 in., 4.44 kN = 1 kip).

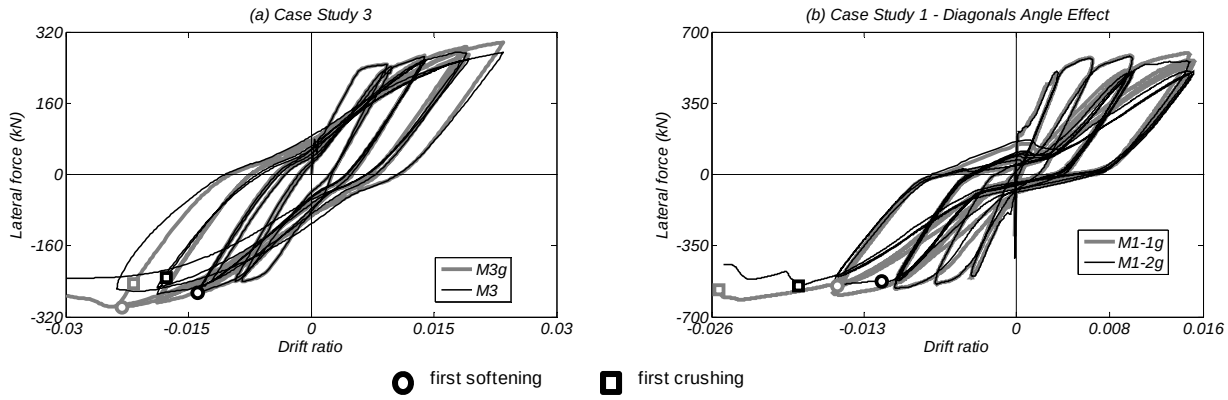

Figure 15. (a) Effect of gage length on the computed response of case study 3. (d) Effect of angle of diagonal truss elements for case study 1. Drift ratio computed at 2150 mm (84.6 in.), 5486 mm (216 in.) from base of wall specimens for Case Studies 1 and 3, respectively. (25.4 mm = 1 in., 4.44 kN = 1 kip, 1MPa = 6.89 ksi).